Optik - International Journal for Light and Electron Optics 282 (2023) 170850

Contents lists available at ScienceDirect

Optik

journal homepage: www.elsevier.com/locate/ijleo

Improvement of the electronic, mechanical and optical properties of cubic As-doped BN alloy for energy harvesting applications

Moaid K. Hussain [a,*], Hayder Salah Mohammed [b]

[a] Department of Electrical Power Techniques Engineering, Al-Hussain University College, Karbala 56001, Iraq
[b] Department of Electrical Power Techniques Engineering, Technical College Al-musaib, Al-furat Al-awsat Technical University, Iraq

ARTICLE INFO

Keywords:
Boron arsenide nitride
Elastic properties
Optical properties
III-V semiconductors
Optoelectronics

ABSTRACT

The electronic structure, elastic and optical properties with wide energy band gap (E_g) in mixed crystal semiconductors containing As-doped BN are reported. Density functional calculations (DFT) were performed for comprehensive detection and understanding of structural, optoelectronic, and elastic properties for mixed semiconductors in the cubic phase. When applying Vegard's law for As, BN, and mixed alloys based on $BN_{1-x}As_x$, where x = 0, 0.25, 0.5, 0.75, and 1, we observed that the distortion of the lattice constants was slight to different condensations. Calculations of E_g values found that the values decreased with an increase in (x) condensation. The bulk modulus, and other elastic parameters were computed and confirmed that the alloys are mechanically stable. The calculations of dielectric Ɛ(ω), refractive index n(ω), higher absorption α(ω) peaks, and other coefficients confirm that $BN_{1-x}As_x$ alloys are favourable for practical photovoltaics. The results confirm that mixed semiconductors have great interest in next-generation optoelectronic devices. This work provides a route for optoelectronic applications.

1. Introduction

Materials such as oxides and III-V semiconductors are necessary for optoelectronic applications. Such materials have essential properties; they are optically translucent to visible light and have considerable electrical conductivity, which makes mixed alloy semiconductors very useful in solar cells and other devices [1-7]. The crucial characteristics of optoelectronic devices based on semiconductor alloys are fundamentally pertinent in designing such device systems. The design and analysis of these devices critically depend on the values of the real and imaginary dielectric parameters (ϵ_r and ϵ_{im}), optical conductivity σ(ω), n(ω), and other optical properties [8-12]. The structure of III-V materials consists of a cubic mineral, sphalerite, or wurtzite based on a hexagonal structure [13]. III-boron semiconductor alloys (with As, N, and In) have recently attracted significant attention. The first motivation for studying these materials comes from their energy band gaps ranging from 1.5 to 6.5 eV and their high bonding power. Therefore, these alloys are often used in light-emitting applications and significant-temperature transistors. The $GaAs_{1-x}Sb_x$ alloy is one of the III-V semiconductors and contains GaAs and GaSb alloys utilised in optoelectronic applications [14]. These compounds have an E_g that ranges from near 0.9–1.55 eV for the GaAs and GaSb and have high α(ω) properties that are beneficial for photovoltaic systems. Another example investigated is BN_xP_{1-x} mixed with two binary alloys, BP and BN. It is found that the E_g ranges between 2.07 and 6.4 eV, and optical properties were computed. They found that ϵ (ω), n(ω), loss-energy L(ω), extinction k(ω), reflectivity R(ω), and α(ω) parameters move towards higher energies. The cubic binary boron nitride (BN) and boron arsenide (BAs) have E_g near 1.5–1.9 eV and (5.2–6.6) eV,

* Corresponding author.
E-mail address: moaid222000@yahoo.com (M.K. Hussain).

https://doi.org/10.1016/j.ijleo.2023.170850
Received 20 December 2022; Received in revised form 29 March 2023; Accepted 2 April 2023
Available online 7 April 2023

respectively. These alloys were found in previous calculations to have good electrical conductivity, which is considered essential for optical devices. Both alloys have good permeability over a vast range between ultraviolet (UV) and visible. Previous studies that calculated elastic parameters showed that BN and BAs are mechanically stable. Calculations of their optical and thermodynamics parameters confirm that BN and BAs alloys are suitable for thermoelectric and optoelectronic applications due to their high absorption and large E_g. For optoelectronic systems, the active compounds are grown by forming thin films on supports. The lattice constant difference and variance in thermal parameters between the layers and supports may lead to significant stresses in the upper layer's structure. Therefore, it is indispensable to calculate their elastic parameters, which describe their response to applied pressure. This paper investigates mixed cubic $BN_{1-x}As_x$ alloys in the DFT field [15-19]. Both binary BN and BAs alloy create $BN_{1-x}As_x$, where x denotes the molar fraction. We compute the influence of doping As atoms on the structure and properties of $BN_{1-x}As_x$. These calculations indicate that new properties can be obtained, which may reveal $BN_{1-x}As_x$ to be useful in designing optoelectronic devices. The calculations of our work prepare data for future experimental works on $BN_{1-x}As_x$.

2. Method of calculations

We applied DFT calculations using the Wien$_2$k code to calculate the characteristics of BAs, BN, and doping alloys [20,21]. The value of the cut-off for valence electrons was as specified 500 eV, execution of expansion for the electronic wave function in the case of Vanderbilt's ultra-soft pseudo-potential. Electronic exchange-correlation effects were characterised using Perdew–Burke–Emzerhof-(PBE) method based on a general gradient approximation (GGA) approach to explore specific properties of doping compound [22-24]. Our calculations use GGA with an applied Tran–Blaha-modified Becke–Johnson (TB-mBJ) path. A k-points of 12 × 12 × 12 were selected for BAs, BN, and the doping alloy. Broydene Flectchere Goldfarbe Shenno (BFGS) algorithm was employed to evaluate atom relaxation to energies of 0.00003 eV per atom, and the entire energy concourse is 0.06 eV per Å. BAs and BN binary model after some selective As atom impurity using order selected by frequently repeated terms. The binary BN and BAs have a structure belonging to the space group 216 F-43 m while doped $BN_{0.75}As_{0.25}$ and $BN_{0.25}As_{0.75}$ have a structure belonging to the space group 215 P-43 m. The structure of $BN_{0.5}As_{0.5}$ belongs to the space group 115 P-4 m2. We can transform this tetragonal into the cubic group by SQS or SAE whose information description can be described in Refs. [10,25]. The $BN_{1-x}As_x$ were modelled at (x = 0.25, 0.5, and 0.75) with ordered structures designed in terms of periodically repeated supercells with the primitive cell of BN to a 2×2x 2 consisting of 32 atoms (B and N consist of both 16 atoms) and used the supercell to simulate As-doped systems. Structural optimization was implemented by minimizing the total energy of the cell constants and atomic positions. Charpin was used to determine the optical properties for BAs, BN, and the doping alloy using a random phase approximation (RPA) method [26]. The dielectric function for the alloy was computed by using $\epsilon_1(\omega)$ and $\epsilon_2(\omega)$ components, determined by transition frequency within the valence band (VB) and conduction band (CB) states. These relations are shown below:

$$\epsilon\ (\omega) = \epsilon_1(\omega) + \epsilon_2(\omega)$$

In computations of the elastic constants, accurate single-alloy elastic constants C_{ij} were received from the DFT of the unit cell absolute energy difference as a role of particular lattice constant distortions. When checking the accuracy of the C_{ij} numerical evaluation of the materials, we used two sets of distortions for the ground state unit cell, developed by Charpin and integrated it in the Wien$_2$k package [26]. In cubic symmetry, only three elastic parameters (C_{11}, C_{12}, and C_{44}) were applied. The C_{11} determines the stiffness against principal strains as[27-34]:

$$C_{11}\text{-}\ C_{12} > 0;\ C_{11} > 0;C_{11}2\ + C_{12} > 0$$

$$C_{12} < B < C_{11};\ C_{44} > 0$$

Young's modulus (Y)was calculated based on the bulk modulus (B), pressure (C"), hardness (Hυ), Kleinman internal strain (ζ), and elastic anisotropy factor (A) of alloys calculated using the relations.

$$Y = 9BG\ /\ (3B + G)$$

$$C" = C_{12}–C_{44}$$

$$H\upsilon = 0.92(G/B)^{1.137}G^{0.708}$$

$$\zeta = \left(\frac{8C_{12} + C_{11}}{2C_{12} + 7C_{11}}\right)$$

$$A = \left(\frac{C_{44}}{C_{11} - C_{12}}\right)$$

3. Results and discussion

3.1. Structural and electronic properties

The ground state parameters for x = 0.0, 0.25, 0.50, 0.75, and 1were calculated using the Murnaghan equation [35]. The optimised

lattice was constant for x = 1 and x = 0.0, equal to 4.81 Å and 3.61 Å, respectively, which agrees with other studies [36-48]. The lattice parameters of x = 0.0, 0.25, 0.50, 0.75, and 1 are listed in Table 1. No data about these alloys have been published before. The semiconductor material calculations show that the lattice constant deviation obeys Vegard's law [49-51,12]. This law assumes the location of atoms at particular lattice sites, and the lattice constant varies linearly after inserting the composition x. The calculation results (Fig. 1) show lattice constants vary linearly approximately with x values. Based on the cubic phase, we calculated and analysed the total density of states (DOS) and partial density of states (PDOS) to analyse participation for different levels of B, N, and As atoms. We observed that the structure on the lower-lying energy side of the DOS consisted of a peak located at a close range between 5.5 and 12.5 for all x concentrations. There are other individual peaks due to states of the B 3p, N 4p and As 3 s. The substitution of the N atom by an As atom leads to a change in the As-s position, indicating that part of N-s. DOS and PDOS show three major peaks named VB referring to s, VB' to B-d, and VB" to the B-s and P states. Also, the lower region in the CB due to B-s and P states could be noted. We calculated the E_g since this value is critical to better understand the performance of semiconductor optoelectronic devices. The results are listed in Table 2. The band structure calculations of the alloys were implemented after the first relaxation of the positions of atoms. Second, implement with high symmetry positions in the first BZ in cubic phase as presented in Fig. 2. We note that the VBM and CBM for all $BN_{1-x}As_x$ are found at the Γ point, which creates a direct E_g. A direct E_g could be observed in the range of x = 0 to x = 1 of 6.12–1.82 eV, which agrees with other studies as shown in Table 2. When substitution of the N atom by an As atom, the lower part of the VB is dominated by N-d states, and the upper part of the N is dominated by As-p and N-d states, while the lower part of the CB is dominated by B-s and N-p states. Therefore, the $BN_{1-x}As_x$ may be optically active in the visible range. The existence of this property can be considered a desirable factor for using this material in optoelectronic applications.

3.2. Elastic properties

In technological compounds, elastic characteristics play a prominent role. Lagrangian proposed an elasticity theory in which they calculated elastic properties as an anisotropic and homogeneous elastic median. The mechanical characteristics can be determined from elastic constants, which comprise primary data about the natural forces of these compounds. These characteristics then fulfil applications related to mechanical nature, like elastic stress, load deflection, and other applications. The mechanical properties of $BN_{1-x}As_x$ were calculated using Born-Huang (BH) criteria stability. We found that BH easily achieved values for these constants. The $BN_{1-x}As_x$ alloy was found to be stab, according to the calculated mechanical properties. The Band G values depend on approximating Voigt-Reuss-Hill criteria (VRH). The G and B values are listed in Table 3. The ratio(known as the Pugh ratio (Pr) between G and B for x = 0, 0.5, 0.75, and 1 is less than 1.75, meaning the material is brittle. The Pr value for x = 0.25 is greater than 1.75, so the material is ductile. The calculation result of (V) confirms the brittle property of x = 0, 0.5, 0.75, and 1 due to the V value being lesser than the condition value (0.25), while for x = 0.25 found to be more than 0.25 and confirms ductile property. The C" value determines the ductility and brutality of alloys. The values of C" are negative for alloys where x = 0, 0.5, 0.75, and 1, which confirms their brittle nature. The C" value for x = 0.25 supports ductile nature. The Hυ value can be used as a reference for experimental computations due to improvements in G and B macroscopic connotations. For the allows examined, Hυ lies within values ranging from 25 to 61 GPa for x = 0, 0.25, 0.5, 0.75, and 1. The ζ value for x = 0, 0.25, 0.5, 0.75, and 1 ranges between 0.37 and 0.61. Due to this range and where ζ does not equal 0, bond bending is reduced, which means the internal displacement within the compounds is small. The A value determines the potential of coaxing microcracks in the alloys. A = 1 for x = 0, 0.25, 0.5, 0.75, and 1; therefore, the nature of alloys is isotropic, but when A not equal to 1 means the alloy is anisotropic.

3.3. Optical properties

Studying the optical properties of semiconductor compounds is vital for practical device systems such as solar cells and photodetectors. The relationship between electronic structure and optical properties of semiconductor alloys was calculated. The calculated

Table 1
The calculated lattice constants a_o(Å) of $BN_{1-x}As_x$ alloy.

Compositions x	a (Å) This work	a (Å) Previous Studies	
		EXP.	DFT
0.0	3.61	3.61[40]	3.62[40]
		4.61[48]	3.615[48]
		3.616[43]	3.62[43]
		3.627[41]	3.61[39]
		3.61[39]	3.62[47]
			3.61[45]
0.25	3.95	-	-
0.5	4.20	-	-
0.75	4.41	-	-
1.00	4.81	4.78[42]	4.77[37]
		4.77[37]	4.77[36]
		4.77[47]	4.81[47]

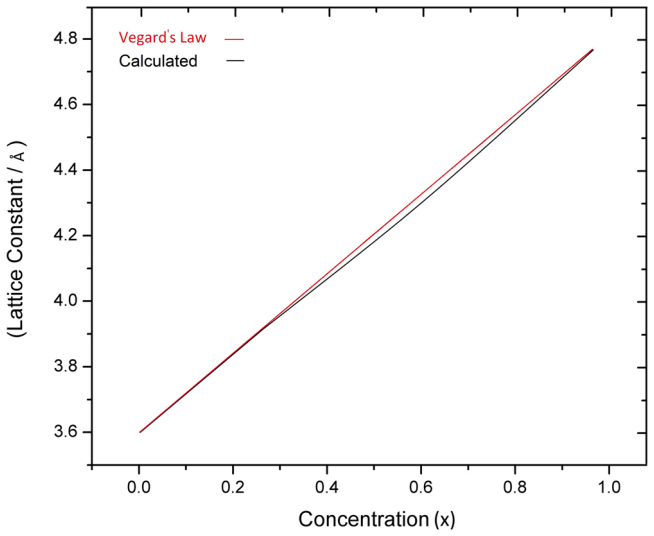

Fig. 1. The variation of the calculated lattice constants with change in x for $BN_{1-x}As_x$ alloy.

Table 2
The calculated energy gap (Eg) of BN1-xAsx alloy.

Compositions x	Eg (eV) This work		Eg (eV) Previous Studies	
	TB-mBJ	PBE-GGA	DFT	EXP.
0.0	6.12	5.95	6.40[40]	6.10[40]
			6.60[41]	5.00[48]
0.25	5.9	5.5	-	-
0.5	3.6	3.2	-	-
0.75	2.4	2.90	-	-
1.0	1.82	1.64	1.69–189[37]	2.02[46]
			1.84[42]	1.82[42]
			1.62[44]	1.77[37]

values for $\epsilon1(\omega)$ and $\epsilon2(\omega)$ are shown in Fig. 3. The values of $\epsilon1(\omega)$ and $\epsilon2(\omega)$ behaved in the same way when the alloy moved between transitions within x = 0, and x = 1, and this behaves similarly in III-V bonded semiconductor compounds, where the main difference determines the transition energies. The high peak of $\epsilon1(\omega)$ for x = 0 appears at 9.8 eV, and x = 1 near E ≈ 7.3 eV, as shown in Fig. 2(a). When the compound x (0−1) changes, the peaks shift to different energy values, 4.8 eV and 4.7 eV for x = 0.25 and 0.5, respectively. For an alloy where x = 0.75, the high value of $\epsilon1(\omega)$ of 10 eV is due to assigned inter-state transitions. Fig. 2(a) shows $\epsilon1(\omega)$ for x = 0, where there is a resonant frequency at 10.5 eV; changes in resonant frequencies are found at 4.5 eV for x = 0.25 and x = 0.5 and reaches 10.1 eV for x = 0.75 and 7.5 eV for x = 1. In $\epsilon2$ (ω), prominent peaks are presented in $BN_{1-x}As_x$ at x = 1, and other x almost have the same peak. They begin from the Γ with type of E_0 transition, which corresponds to standards of E_g and dramatic increase reach to $\epsilon2 \approx 26$ about 8.5 eV for x = 1. This increase in $\epsilon2$ case to begin transitions of direct inter-band in Γ with high BZ symmetry. The $\epsilon2$ value barely shifts to a lower value near 20 eV. This reverted to bands which originated mainly from bands at Γ point. When moving x = 0 to x = 1, all peaks change. The main difference in $\epsilon2$ (ω) at (x) returns to energies transition. The α(ω) provides more information about the characteristics of light permeation of particular wavelengths to materials before absorbing light. Also, influences of optical properties on optoelectronic devices concern α (ω). Fig. 2(c) presents this parameter with respect to E_{Ph}. For x = 0 and x = 0.75, we find high peaks of absorption spectra that reach more than 5×10^5 at a range between 11 and 15 eV. When x = 0.25 and 0.5, the high peaks reach more than 3×10^5 at 8 eV, while when x = 1 reach more than 4×10^5 at 6 eV. This means the peaks of absorption spectra varied between x = 0 and x = 1.

The light absorption of x = 0.25, 0.5 and 1 was poor compared with x = 0 and x = 0.75 due to sharing the electrons at the VB edge only in absorption. When E_{ph} increased at x = 0 and x = 0.75, the α (ω) which led to increased interaction with photons and caused an increase in absorbed photons. Peaks between x = 0 and x = 1 in the low energy region show a red shift. This finding makes $BN_{1-x}As_x$ more important in the short-wave IR range in infrared optoelectronic systems. The n(ω) values from x = 0 to x = 1 were calculated; The peaks, as shown in Fig. 3(d), constructed from exciting transitions in the E_0 range, could be observed. The peaks vary in intensity between x = 0 and x = 1; the higher peaks are found at x = 1 at 5.1 eV. The significant peak in $n(\omega)$ corresponds to a two-dimensional (2D) excitation transition E_1. The higher static n(ω) was calculated to be 3.2 for x = 1, and the lower one is 2.2 at x = 0. The k(ω) displays a similar trend as $\varepsilon_2(\omega)$. The k(ω) values are shown in Fig. 2(e). The major peak values for x = 0.0, 0.25, 0.5, 0.75 and 1 are

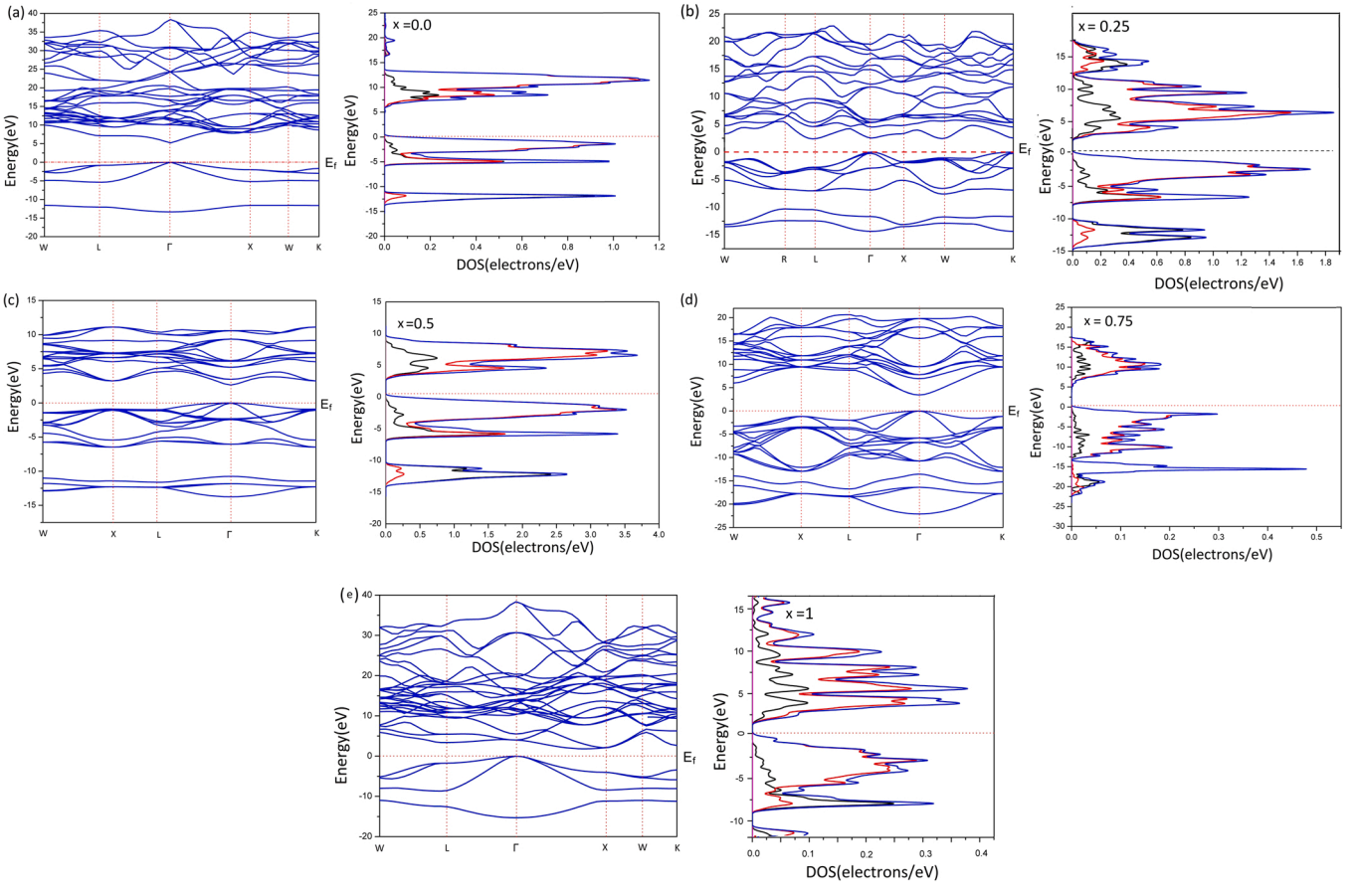

Fig. 2. The band structure and density of states of the $BN_{1-x}As_x$ alloy where (a) x = 0, (b) x = 0.25, (c) x = 0.5, (d) x = 0.75 and (e) x = 1.

Table 3
The calculated elastic characteristics of BN1-xAsx alloy.

parameters	Compositions X = 0.0	Compositions X = 0.25	Compositions X = 0.5	Compositions X = 0.75	Compositions X = 1
C_{11}	817 813[48] 680[41] 781[47] 798[33]	2337	997	523	292 285[42] 275[44] 275[37] 267[47]
C_{12}	181 185[48] 229[41] 190[47]	1145	420	121	84 79.5[42] 71[44] 73[37] 64[47]
C_{44}	471 450[48] 405[41] 442[47]	934	575	264	155 149[42] 170[44] 168[37] 162[47]
B	372 369–372[40] 374–400[48] 375–402[43] 382[41] 375[39,47] 392[45]	1542	1071	255	152 148[42] 139[44] 139[37] 138[47]
β	0.0026 0.019[41]	0.0006	0.0009	0.004	0.005
G	399 394[48] 405–412[43] 407[45]	761	713	234	131 128[42] 138[44] 134[47]
E	865 875[48] 8554[47] 909[45]	1584	689	477	320 326[42] 312[44] 300[47]
V	0.12 0.11[48] 0.117[5] 0.07[45]	0.32	0.19	0.18	0.23 0.22[42] 0.12[44] 0.11[47]
Pr = B/G	0.93	2.02	1.50	1.08	1.16 0.82[42] 0.96[44]
Hv	60 67[48] 62[45]	45	61	40	25
ζ	0.37 0.36[47]	0.61	0.55	0.38	0.43 0.4[44] 0.93[47]
A	1.48 1.439[47]	1.56	1.99	1.31	1.5 1.67[44] 1.59[47]

observed at 2.6, 2.7, 2.7, 2.3, and 3.7 eV, respectively. Fig. 2(f) represents L(ω) of electrons passing through the compounds and calculated results for $BN_{1-x}As_x$ for various values of x. The peaks in the L(ω) curve show characteristics which correspond to plasma correspond for which similar frequency describes plasma frequency, these different match areas of the reflection range. For small peaks, there is a match with the broad plasma resonance at 11.6 eV at lower energies. When x changes, there is a slight change in the plasma frequencies for lower E_{ph} and a slight change in the observation domain. The result is supposed to be the basic standard in optoelectronic devices using semiconductor compounds. The higher peaks are than 40 at 30 eV for x = 0.75, which means the material is more conductive. The reflectivity parameter R(ω) is considered to be an important parameter in linear optics because of its high sensitivity with respect to groups for ε1(ω) and $\varepsilon_2(\omega)$[52,53]. Fig. 3(g) presents that the upper R(ω) for x = 0.0, 0.25, 0.5, 0.75 and 1 equals 19, 14, 15, 27, and 10 eV, respectively, which determines the UV spectrum. Fig. 3(h) presented the optical conductivity σ(ω). σ(ω) evolves from zero to a maximum value then decreases dramatically to zero because of the system's metallic character. We find high σ(ω) at 15 eV for x = 0, which agrees with the absorption parameter's peak position. The σ(ω) parameter is a purpose for the VB band transition of As(N)-p with CB of B-s level. The higher σ(ω)is calculated between the visible and UV spectrum.

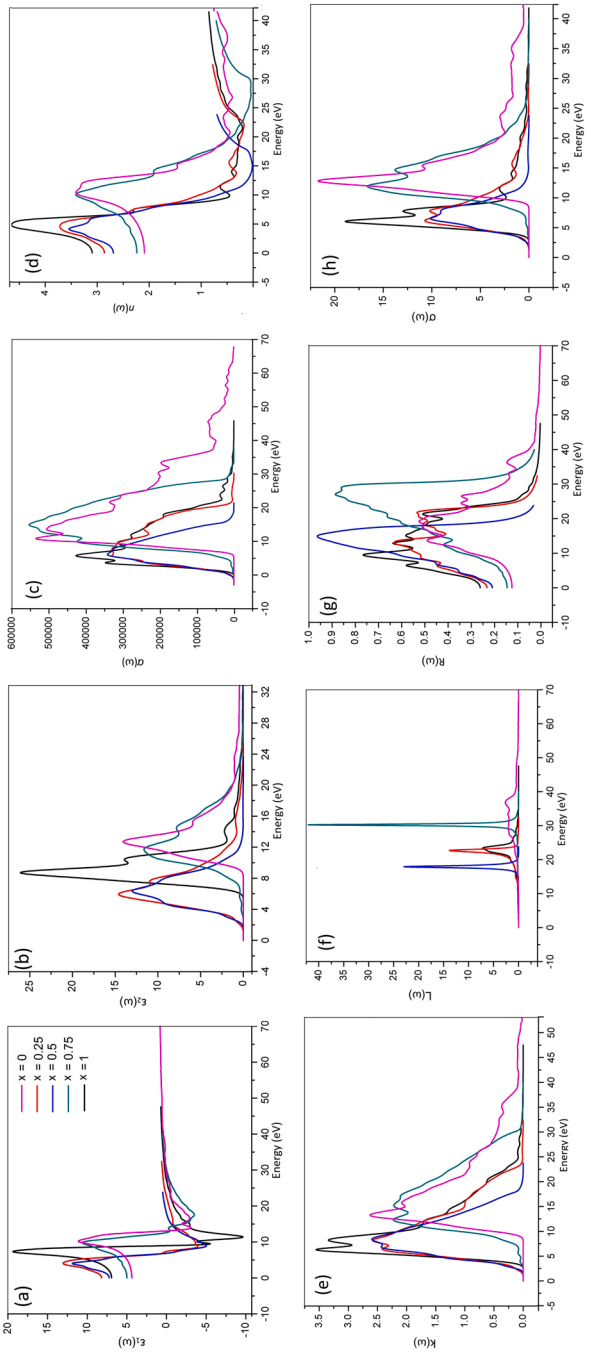

Fig. 3. The optical characteristics of the $BN_{1-x}As_x$ where (a) $\varepsilon_1(\omega)$, (b) $\varepsilon_2(\omega)$, (c) $\alpha(\omega)$, (d) $n(\omega)$, (e) $k(\omega)$, (f) $L(\omega)$, (g) $R(\omega)$, and (h) $\sigma(\omega)$.

4. Conclusion

Based on DFT, we demonstrate the structural, electronic, elastic, and optical characteristics of a series of $BN_{1-x}As_x$ alloys of differing compositions. The calculations of lattice parameter values agreed with previous results and were found to undergo slight variations at different concentrations according to Vegard's law. The E_g decreased with an increase in the proportion of As atoms. The elastic parameters of all x = 0, 0.5, 0.75, and 1 showed mechanical stability, and all alloys were brittle except x = 0.25, which was found to be ductile. Our calculations showed that these compounds have small internal displacement due to the ζ value for x = 0, 0.25, 0.5, 0.75, and 1 ranging between 0.37 and 0.61. The (A) values for all the x values were found to be lesser and greater than 1, which indicates anisotropic property. The G and P_r, and other parameters were computed. The main peak of ϵ_1 (ω) for x = 1 appeared at 7.3 eV, and x = 0 at E .3 s w eV. When the compound x (0−1) changed, peaks shifted at various energies near 5.3 and 5.2 for x = 0.25 and 0.5, respectively, while at a higher value near 10.2 at x = 0.75 due to assigned inter-state transitions. The absorption calculations demonstrate that $BN_{1-x}As_x$ have a higher peak reaching more than 5×10^5 for x = 0.0 and 0.75. The maximum R(ω) for x = 0.0, 0.25, 0.5, 0.75, and 1 equals 19, 14, 15, 27, and 10 eV, respectively, which determines the UV spectrum. The peaks demonstrate transitions between the VB and CB inter-bands. The calculations of optical coefficients confirm that $BN_{1-x}As_x$ is appropriate for photovoltaic systems. This paper suggests routes for subsequent experimental works in optoelectronic applications.

Declaration of Competing Interest

The authors declare the following financial interests/personal relationships which may be considered as potential competing interests: Moaid K Hussain reports was provided by Alhussain University College. Moaid K Hussain reports a relationship with Alhussain University College that includes: employment. Moaid K Hussain has patent pending to Optik. Hayder Salah Mohammed.

Data Availability

No data was used for the research described in the article.

References

[1] M.A. AliG, M. Laref, Exploring the ferromagnetic half metallic nature of Cs2NpBr6 via spin polarized density functional theory, Chin. Phys. B 29 (2020) 6, https://doi.org/10.1088/1674-1056/ab7da4.

[2] K. Boudiaf, A. Bouhemadou, O. Boudrifa, K. Haddadi, F. Saad Saoud, R. Khenata, Y. Al-Douri, S. Bin-Omran, M.A. Ghebouli, Structural, elastic, electronic and optical properties of LaOAgS-Type silver fluoride chalcogenides: first-principles study, J. Electron. Mater. 46 (2017) 4539–4556, https://doi.org/10.1007/s11664-017-5452-6.

[3] M. Daouahi, N. Rekik, Effect of substrate temperature on (Micro/Nano)structure of a-SiC:H thin films deposited by radio-frequency magnetron sputtering, J. Phys. Chem. C. 116 (39) (2012) 21018–21026, https://doi.org/10.1021/jp3079937.

[4] M. Daouahi, M. Omri, A. Kerm, F.A. Al-Agel, N. Rekik, An investigation on the effect of high partial pressure of hydrogen on the nanocrystalline structure of silicon carbide thin films prepared by radio-frequency magnetron sputtering, Spectroc. Act. A: Molec. Biomol. Spectr. 136 (2015) 1409–1417, https://doi.org/10.1016/j.saa.2014.10.029.

[5] L. Hasni, M. Ameri, D. Bensaid, I. Ameri, S. Mesbah, Y. Al-Douri, J. Coutinho, First-principles calculations of structural, magnetic electronic and optical properties of rare-earth metals TbX (X=N, O, S, Se, J. Supercond. Nov. Magn. 30 (2017) 3471–3479, https://doi.org/10.1007/s10948-017-4130-5.

[6] S. Saib, N. Bouarissa, The effect of pressure on band parameters and optical characteristics in indium nitride, J. Electron. Mater. 51 (2022) 3758–3765, https://doi.org/10.1007/s11664-022-09624-5.

[7] S.V. Syrotyuk, M.K. Hussain, The effect of Cr impurity and Zn vacancy on electronic and magnetic properties of ZnSe crystal, Phys. Chem. Solid State 22 (2021) 529, https://doi.org/10.15330/pcss.22.3.529-534.

[8] M. Al-Douri, A. Ameri, K.M. Bouhemadou, Batoo, first-principles calculations to investigate the refractive index and optical dielectric constant of Na_3SbX_4 (X = S, Se) ternary chalcogenides, Phys. Status Solidi B (2019) 1900131, https://doi.org/10.1002/pssb.201900131.

[9] A. Khireddine, A. Bouhemadou, S. Alnujaim, N. Guechi, S. Bin-Omran, Y. Al-Douri, R. Khenata, S. Maabed, A.K. Kushwaha, structural, electronic, optical and elastic properties of the zintl-phases AE_3GaAs_3 (AE = Sr, Ba), Sol. Sta. Sci. 114 (2021), 106563, https://doi.org/10.1016/j.solidstatesciences.2021.106563.

[10] M. Rashid, M. Jamil, Q. Mahmood, S.M. Ramay, A. Mahmood, H.M. Ghaithan, *Ab-initio* calculations of band gap tuning of $In_{1-x}Ga_xY$ (Y = N, P) alloys for optoelectronic applications, Chin. Phys. B 30 (2) (2021), 026301, https://doi.org/10.1088/1674-1056/abc0db.

[11] S. Saib, N. Bouarissa, The effect of pressure on band parameters and optical characteristics in indium nitride, J. Electron. Mater. 51 (2022) 3758–3765, https://doi.org/10.1007/s11664-022-09624-5.

[12] R. Xingxiang, Z. Fuchun, Z. Weihu, First-principles investigation on electronic structure and optical properties of wurtzite $In_xGa_{1-x}N$ alloys, Rare Met. Mater. Eng. 44 (2015) 12, https://doi.org/10.1016/S1875-5372(16)60044-9.

[13] M. Shakila, M. KashifMasooda, M. Zafarb, Shabir Ahmad, A. Hussain, M.A. Gadhi, S.A. Buzdar, T. Iqbal, Theoretical study of structural, electronic and optical properties of $In_xGa_{1-x}N$ alloys, Optik 174 (2018) 739, https://doi.org/10.1016/j.ijleo.2018.08.083.

[14] S. Gaguia, S. Ghemidc, H. Meradjic, B. Zaidid, B. Amimourc, S.A. Tahire, R. Ahmede, B. Chouialb, B. Hadjoudjab, A.K. Kushwah, Ab-initio study on the phase transition, elastic, optoelectronic, and thermodynamic properties of $GaAs_{1-x}Sb_x$, Optik 219 (2020), 165253, https://doi.org/10.1016/j.ijleo.2020.165253.

[15] Y. Benkaddour, A. Abdelaoui, A. Yakoubi, H. Khachai, Y. Al-Douri, S. Bin Omran, A. Shankar, R. Khenata, C.H. Voon, Deo Prakash, K.D. Verma, First-principle calculations of structural, elastic, and electronic properties of intermetallic rare earth R_2Ni_2Pb (R = Ho, Lu, and Sm) compounds, J. Supercond. Nov. Magn. 31 (2018) 395–403, https://doi.org/10.1007/s10948-017-4234-y.

[16] K. Bidai, M. Ameri, S. Amel, I. Ameri, Y. Al-Douri, D. Varshney, C. Voon, First-principles calculations of pressure and temperature dependence of thermodynamic properties of anti-perovskite $BiNBa_3$ compound, Chin. J. Phys. /55 5 (2017) 2144–2155, https://doi.org/10.1016/j.cjph.2017.03.023.

[17] M.K. Hussain, Investigations of the stability, electronic and magnetic structures in the Zr_2Ni-based Heusler compounds: First principles study, Mater. Sci. Eng. B 264 (2021), 114922, https://doi.org/10.1016/j.mseb.2020.114922.

[18] M.K. Hussain, K.I. Inad, Theoretical study of surface properties of new (0 0 1)- and (1 1 1)-surface YCoCrGe quaternary Heusler compounds, Thin Solid Films 663 (2018) 100, https://doi.org/10.1016/j.tsf.2018.08.017.

[19] K.H. Moaid, G.Y. Gao, K.L. Yao, Investigations of the electronic and magnetic structures at Heusler alloy surface: Co_2TiGe (0 0 1), J. Electron. Spectrosc. Relat. Phenom. 203 (2015) 45–50, https://doi.org/10.1016/j.elspec.2015.05.015.

[20] M.K. Hussain, Investigations of the electronic and magnetic properties of newly(001) surface LiCrS and LiCrSe half-Heusler compounds, Appl. Phys. A 124 (2018) 343, https://doi.org/10.1007/s00339-018-1760-9.

[21] M.K. Hussain, F.H. Abdulsadah, M.M. Ali, Half-metallic properties of the new Zr_2RhB inverse Heusler alloy with $CuHg_2Ti$–type structure, Mater. Today Proc. 18 (2019) 2590–2594, https://doi.org/10.1016/j.matpr.2019.07.117.

[22] M. Hussain, G. Gao, K. Yao, Half-Metallic properties in the new Ti_2NiB heusler alloy, J. Supercond. Nov. Magn. 28 (2015) 3285, https://doi.org/10.1007/s10948-015-3149-8.

[23] M. Hussain, G. Gao, K. Yao, Half-metallic properties of the new Ti $_2$YPb(Y = Co,Fe) Heusler alloys, Int. J. Mod. Phys. B 29 (2015) 1550175, https://doi.org/10.1142/S0217979215501751.

[24] K. Moaid, Half-metallicity of bulk and (001) surface in the Co_2FeGa Heusler compound: a theoretical study, Surf. Rev. Lett. 4 (2019) 1950130, https://doi.org/10.1142/S0218625×19501300.

[25] F. Tian, D.Y. Lin, X. Gao, Y.F. Zhao, H.F. Song, A structural modeling approach to solid solutions based on the similar atomic environment, J. Chem. Phys. 153 (2020), 034101, https://doi.org/10.1063/5.0014094.

[26] T. Charpin, 2001. (see $WIENROOT/SRC/elast-UG.ps). C. Blaha, Schwarz, K., Madsen, G. K. H., Kuasnicka, D. and Luitz, J., WIEN2k, An augmented plane wave +local orbitals program for calculating crystal properties, K. Schwarz Technical Universitat, Wien, Austria, ISBN 3–9501031-1–2 (2001).

[27] M.H. Benkabou, M. Harmel, A. Haddou, A. Yakoubi, N. Baki, R. Ahmed, Y. Al-Douri, S.V. Syrotyuk, H. Khachai, R. Khenata, C.H. Voon, Structural, electronic, optical and thermodynamic investigations of NaXF3 (X= Ca and Sr): first-principles calculations, Chin. J. Phys. 56 (2018) 131–144, https://doi.org/10.1016/j.cjph.2017.12.008.

[28] A. Bouhemadou, D. Allali, K. Boudiaf, B. Al Qarni, S. Bin-Omran, R. Khenata, Y. Al-Douri, Electronic, optical, elastic, thermoelectric and thermodynamic properties of the spinel oxides $ZnRh_2O4$ and $CdRh_2O4$, J. Alloy. Comp. 774 (2019) 299–314, https://doi.org/10.1016/j.jallcom.2018.09.338.

[29] M.K. Hussain, Effects of strain on the half-metallic and elastic properties of FeCrTe and CoCrSi with Clb structure, SPIN 9 (2019) 1950018, https://doi.org/10.1142/S2010324719500188.

[30] M.K. Hussain, Kl Yao, Spin polarization calculations and related properties of the surfaces of CoVTe alloy and interface with a BeTe semiconductor, Appl. Phys. Mater. Sci. Process 125 (2019) 463, https://doi.org/10.1007/s00339-019-2752-0.

[31] M.K. Hussain, O.T. Hassan, A.M. Algubili, Investigations of the electronic and magnetic structures of Zr_2NiZ (Z= Ga, In, B) Heusler compounds: first principles study, J. *Electron. Mater.* 47 (2018) 6221, https://doi.org/10.1007/s11664-018-6512-2.

[32] M.K. Hussain, M.J. Alwazzan, R. Paudel, 111),(001), and (110) surface effects on the stability and electronic-magnetic properties of Mn_3P alloy, Phys. E 131 (2021), 114717, https://doi.org/10.1016/j.physe.2021.114717.

[33] M.K. Hussain, S.R. Saeed, M.R. Saeed, S. Syrotyuk, Surface effects on the electronic and optical properties of the Mn_3P alloy for optoelectronic applications, Optik 242 (2021), 166667, https://doi.org/10.1016/j.ijleo.2021.166667.

[34] K.H. Moaid, N.A. Asmaa, Stability, electronic-magnetic, dynamical and optical properties of the Mn_3P alloy based on the $D0_3$-Type, Optik 226 (2021), 165948, https://doi.org/10.1016/j.ijleo.2020.165948.

[35] K. Radja, B.L. Farah, A. Ibrahim, D. Lamia, I. Fatima, B. Nabil, A. Mohamed, Y. Al-Douri, A.A. El-Rehim, Investigation of structural, magneto-electronic, elastic, mechanical and thermoelectric properties of novel lead-free halide double perovskite Cs2AgFeCl6: First-principles calcuations, J. Phy. Chem. Solids 167 (2022), 110795, https://doi.org/10.1016/j.jpcs.2022.110795.

[36] B. Bouhafs, M. Ferhat, Electronic structure theory of unusually matched $BAs_{1-x}P_x$ alloys using high throughputab-initio computation, Phys. B 24 (2019), 411901, https://doi.org/10.1016/j.physb.2019.411901.

[37] J. Buckeridge, D. Scanlon, The electronic band structure and optical properties of boron arsenide, Phys. Rev. Mater. 3 (2019) 05160, https://doi.org/10.1103/PhysRevMaterials.3.051601.

[38] K. Bushick, S. Chae, Z. Deng, J.T. Heron, E. Kioupakis, Boron arsenide heterostructures: lattice-matched heterointerfaces and strain effects on band alignments and mobility, npj Comp. Mater. (2020) 3, https://doi.org/10.1038/ s41524-019-0270-4.

[39] P. Chakra, b Guoping, X. LeiCao, Y. Wang, Lattice thermal transport in superhard hexagonal diamond and wurtzite boron nitride: A comparative study with cubic diamond and cubic boron nitride, Carbon 139 (2018) 85–93, https://doi.org/10.1016/j.carbon.2018.06.025.

[40] M. Dadeetan, B. Kianisadr, H. Nejatipour, First principles investigation of the optical properties of BN_xP_{1-x} ($0 \leq x \leq 1$) boron ternary alloys, J. Electron. Mater. 44 (2015) 2699–2711, https://doi.org/10.1007/s11664-015-3691-y.

[41] C. Huang, B. Yang, X. Peng, S. Chen, Plastic deformation and hardening mechanisms of a nano-twinned cubic boron nitride ceramic, ACS Appl. Mater. Interfaces 12 (2020) 50161–50175, https://doi.org/10.1021/acsami.0c.

[42] J.S. Kang, et al., Basic physical properties of cubic boron arsenide, Appl. Phys. Lett. 115 (2019), 122103, https://doi.org/10.1063/1.5116025.

[43] A. Nagakubo, H. Ogi, H. Sumiya, K. Kusakabe, M. Hirao, Elastic constants of cubic and wurtzite boron nitrides, Appl. Phy. Lett. 102 (2013), 241909, https://doi.org/10.1063/1.4811789.

[44] A. Rastogi, P. Rajpoot, U. Verma, Properties of group III–V semiconductor: BAs, Bull. Mater. Sci. 42 (2019) 112, https://doi.org/10.1007/s12034-019-1758-8.

[45] V.L. Solozhenko, V. Bushlya, J. Zhou, Mechanical properties of ultra-hard nanocrystalline cubic boron nitride, J. Appl. Phy. 126 (2019), 075107, https://doi.org/10.1063/1.5109636.

[46] B. Song, K. Chen, K. Bushick, K.A. Mengle, F. Tian, G.A. Gamage, Z. Ren, E. Kioupakis, G. Chen, Optical properties of cubic boron arsenide, Appl. Phys. Lett. 116 (2020), 141903, https://doi.org/10.1063/5.0004666.

[47] M. Ustundag, M. Aslan, Battal G. Yalcin, The first-principles study on physical properties and phase stability of Boron-V (BN, BP, BAs, BSb and BBi) compounds, Comp. Mater. Sci. 81 (2014) 471–477, https://doi.org/10.1016/j.commatsci.2013.08.056.

[48] Q. Wang, L. Chen, L. Xiong, H.R. Gong, Mechanical and thermodynamic properties of cubic boron nitride from ab initio calculation, J. Phys. Chem. Solids 104 (2017) 276–280, https://doi.org/10.1016/j.jpcs.2017.01.029.

[49] B. Asma, F. Belkharroubi, A. Ibrahim, Structural, mechanical, magnetic, electronic, and thermal investigations of Ag_2YB (Y = Nd, Sm, Gd) full-Heusler alloys, emergent Mater. 4 (2021) 1769–1783, https://doi.org/10.1007/s42247-021-00257-8.

[50] B. Fadila, M. Ameri, D. Bensaid, M. Noureddine, I. Ameri, S. Mesbah, Y. Al-Douri, Structural, magnetic, electronic and mechanical properties of full-Heusler alloys Co_2YAl (Y = Fe, Ti): First principles calculations with different exchange-correlation potentials, J. ofMagn. Magn. Mater. 448 (2018) 208–220, https://doi.org/10.1016/j.jmmm.2017.06.048.

[51] Z. Souadia, A. Bouhemadou, R. Khenata, Y. Al-Douri, Structural, elastic and lattice dynamical properties of the alkali metal tellurides: First-principles study, Phys. B: Cond. Matt. 521 (2017) 204–214, https://doi.org/10.1016/j.physb.2017.07.004.

[52] A. Gassoumi, A.M. Alshehri, N. Bouarissa, Electronic structure and optical response for $Zn_{1-x}Be_x$ Se, Results Phy 12 (2019) 1294–1298, https://doi.org/10.1016/j.rinp.2019.01.027.

[53] K. Hadji, A. Abdiche, F. Soyalp, S. BinOmran, Computational investigations on band structure and optical properties of the $BeSe_xTe_{1-x}$ alloys through the FP-LAPW approach, Optik 130 (2017) 1080–1091, https://doi.org/10.1016/j.ijleo.2016.11.105.